Molecular dynamics simulation of vapor deposited amorphous ice

Ulrich Essmann[a] and Alfons Geiger
Physikalische Chemie, Universität Dortmund, D-44221 Dortmund, Germany

(Received 29 December 1992; accepted 27 April 1995)

We report a molecular dynamics simulation of the vapor deposition of amorphous ice on a cold surface. We compare the obtained structure with neutron scattering data of high and low density amorphous ice formed by pressure induced transformation of crystalline ice. The structure of our vapor deposited ice is intermediate between these two, although closer to high density amorphous ice. Its radial distribution functions resemble the results of a simulation of cluster formation in the gas phase as well as of a recent neutron scattering experiment on vapor deposited amorphous ice. The occurrence of an intermediate structure is also in agreement with a recent electron diffraction study. Structural differences are discussed in terms of the hydrogen-bond network. The amorphous surface layer is deeply fissured, suggesting a high porosity of vapor deposited ice. © *1995 American Institute of Physics.*

I. INTRODUCTION

The structure of amorphous solid water has received great attention because of its importance for the investigation of the structure of liquid water[1] and the relevance for practical problems in cryobiology[2] and astrophysics.[3] For a long time the condensation of water vapor on a cold surface (below 77 K) was the only method for generating amorphous solid water.[1] Various vapor deposition experiments yielded diverging results, obviously due to a strong sensitivity on the experimental conditions.[4] Recently, the observation of a blurred structural transition between a high and low density form of vapor deposited ice has been reported,[5] which may help to understand the previous discrepancies. During the last decade, a variety of other methods have been developed, among them the rapid temperature quenching of liquid water[6–8] and the production of amorphous ice via the compression of ice Ih to high density amorphous (hda) ice,[9] which can be converted to low density amorphous (lda) ice by pressure release and heating.[9] The relationship between the amorphous solids made from bulk water and crystalline ice have been the subject of a recent computer simulation study,[10] however this has not yet been done for the case of the vapor deposited material.

The production of amorphous ice by computer simulation has also been a challenge. Tse and Klein were able to observe the transition from ice Ih to hda ice in a molecular dynamics simulation.[11] In a recent simulation series, Zhang and Buch studied the formation of amorphous ice clusters in the gas phase.[12–14] In a very recent study, Wilson *et al.*[15] attempted to simulate the vapor deposition of hda and lda ice. The aim of the present study is to investigate in a computer simulation the structure of amorphous ice formed by vapor deposition on a substrate surface. This structure will be compared with the structure of amorphous ice formed by simulated rapid quenching of liquid water as well as with the results of various other computational and experimental studies.

[a]Also at Department of Chemistry, University of North Carolina, Chapel Hill, North Carolina 27599.

II. COMPUTATIONAL METHODS

The simulation described below follows as closely as possible the experimental procedure to obtain amorphous solid water by condensing water vapor on a substrate at very low temperatures. In order to avoid nucleation of crystalline ice in these experiments the substrate temperature is fixed well below 150 K,[16] the temperature at which amorphous ice transforms into crystalline ice. The experimental deposition rates are very low, usually on the order of a few mg per h for the whole sample,[16] corresponding to film growth rates of micrometers per hour and less. The substrate consisted of different materials: Cu,[16,17] Cd,[18] and silica glass.[17]

In the present simulation study the temperature of the simulation is maintained in the range in which slow condensation of vapor is known experimentally to produce amorphous ice ($T<100$ K). The substrate is represented by two layers of Lennard-Jones spheres parallel to the (100) plane of a fcc crystal. To achieve a good coupling between substrate and adsorbate, comparable to the above-mentioned materials, Lennard-Jones parameters $\epsilon=9.57\times10^{-21}$ J and $\sigma=2.8$ Å are chosen for the interaction between the substrate atoms. To calculate the interaction between the substrate and the adsorbate, the mixed Lennard-Jones parameters are computed according to the Lorentz–Berthelot rules.[19] The nearest-neighbor distance of the substrate atoms corresponds to the minimum in the Lennard-Jones interaction. A square lattice of five primitive cells of the fcc lattice in the x and y directions is built up. This leads to a total number of 100 Lennard-Jones substrate particles and a box length in the x and y directions of 22.2 Å. Periodic boundary conditions are used in the x and y directions to simulate an infinite plane. A schematic picture of the simulated system is displayed in Fig. 1.

No periodic boundary conditions are used in z direction. From positive z values, new water molecules are inserted into the system. The water molecules are described by the SPC/E model.[20] SPC/E has the advantage that it is a three center model and therefore appropriate for large scale simulations. Moreover, it reproduces the structure of bulk water in reasonable agreement with experiments.[20]

 0021-9606/95/103(11)/4678/15/$6.00

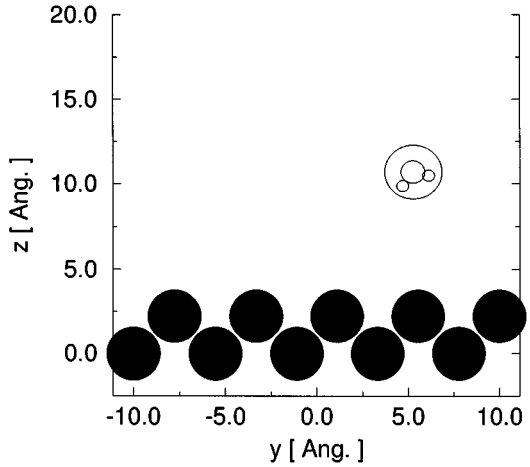

FIG. 1. Cut through the system in $(y\text{-}z)$ direction in the initial stage of the simulation. The substrate atoms (filled circle) are regularly ordered. For the water molecule a sphere, indicating the size of the Lennard-Jones sphere, is drawn together with small circles which indicate the positions of the hydrogen and oxygen atoms. From positive z direction water molecules are inserted at random positions and with random orientations. The initial velocities are towards the surface. Periodic boundaries are applied in x and y direction. Note that the interaction between substrate and adsorbate is only between substrate and oxygen atom of the water molecules since in the SPC/E model only the oxygen atom has a Lennard-Jones interaction.

The SPC/E-pair potential is made up of one Lennard-Jones center and three Coulomb-charge centers per water molecule. It is well known that charges in the vicinity of dielectric walls cause polarization fields, which can be described by image charges. This method would increase the number of interaction centers in the simulation by a factor of 2. To allow longer simulation runs and therefore smaller deposition rates, in closer agreement with experiments, we neglect the image charges and use a cutoff radius $r_c=8.5$ Å for all interactions. To achieve better energy conservation, these interactions are smoothly switched off between $0.95r_c$ and r_c.[21]

Every 2000 molecular dynamics (MD) time steps a new particle is inserted. With an integration step of 2 fs, this corresponds to an interval of 4 ps. In sum total, 500 water molecules were inserted in a simulation of 10^6 time steps. The initial position of each incoming particle is chosen at random just outside the cutoff radius of the other particles. The translational and rotational velocities of the incoming particles obey a Maxwell–Boltzmann distribution of $T=60$ K. The initial direction of the translational velocities is perpendicular to the substrate surface.

The substrate atoms are fixed to the lattice positions via harmonic forces which are present in addition to the Lennard-Jones interactions. In attempting to design the simulation to be as similar as possible to experiments, the temperature control of the system should be achieved by the rescaling of the velocities of the substrate molecules alone. To achieve a good coupling between the water molecules and the adsorbate, the masses of the Lennard-Jones atoms are set to 18 g/mol and the force constant of the harmonic potential to $k=4.72$ kg s^{-2}, leading to a frequency of 2×10^{12} Hz. In this region, a broad band of acoustic phonons can be found in ice.[22] Nevertheless, the simulations showed that the energy which is released during the adsorption of a new molecule, could not be removed fast enough. This led to a temperature increase. This observation is in correspondence to the observation of Biswas *et al.*, who found a similar temperature increase in a simulation of the growth of amorphous silicon.[23] Therefore, we coupled all particles except the last 100 incoming water molecules to an external heat bath of temperature $T=60$ K, according to the method of Berendsen *et al.*[24] (relaxation time $\tau=0.5$ ps).

To monitor the temperature in detail during the simulation, the system is divided into layers parallel to the $(x-y)$ plane. The temperature is computed separately for every layer. The thickness of the layers is chosen in such a way that there are approximately 100 molecules in each layer. Using the method described above, the temperature never exceeds 100 K in any layer during the whole run. However, the temperature in the top layer quite often reaches values close to 100 K. All layers below it stay at a temperature of close to 60 K. The equations of motion are integrated by a quaternion leap-frog algorithm.[25]

In order to estimate to what extent the current results, obtained from the system with 500 water molecules, are sensitive to system size effects, we performed two additional simulations. One simulation with a box length in x and y directions of 17.8 Å and a large simulation with a box length in x and y directions of 35.6 Å. To achieve a similar thickness of the ice layer we performed the small simulation up to a total number of water molecules of 373 and the large simulation up to a total number of 1101 molecules. For the present investigation it is of particular interest that the structure as it is reflected in the pair correlation functions does not show any size effects.

This result is reasonable, if one compares with pure water simulations. From these it is well known that edge lengths of less than 18 Å for the periodic box are sufficient to avoid system size effects on the radial distribution functions. Our systems have this size in the two directions with periodic boundary conditions. In the third, the z direction, the layer of about 40 Å thickness obviously contains a bulk part with a system size independent structure of 19 Å thickness, which we investigated, as described in Sec. V.

The main difficulties of these kind of simulation studies have to be seen in the different time scales of simulations and experiments. The deposition rate of one water molecule per 4 ps on the basis area of 22×22 Å^2, leading to a total simulation run of one million time steps for the 500 molecule system, at first sight seems to be slow on the MD scale. But compared to experimental deposition rates, this is of course many orders of magnitude too fast, leading to the temperature control and energy removal problems, discussed above.

III. TEST OF THE INTERACTION POTENTIAL

Before starting the simulation of the deposition experiments we test the SPC/E potential by determining the structure of bulk liquid water from a simulation at 306 K. The calculated $h(r)$ function, which is a sum of the partial pair

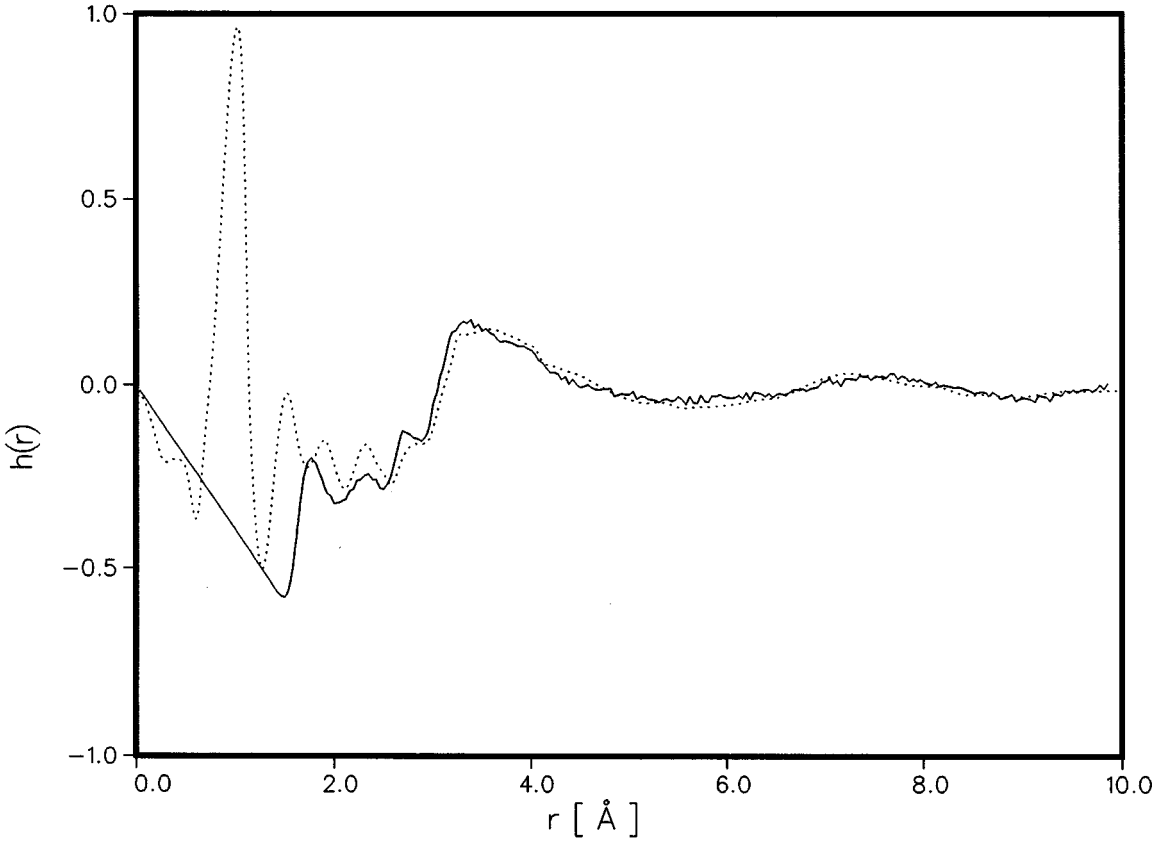

FIG. 2. $h(r)$ function [Eq. (1)] of liquid water. Solid line: simulation at 306 K. Dotted line: experiment at 284 K.

distribution functions, weighted according to the neutron scattering lengths[18] (ρ is the molecular number density), given by

$$h(r)=4\pi r\rho[0.092g_{\mathrm{OO}}(r)+0.422g_{\mathrm{OH}}(r)+0.486g_{\mathrm{HH}}(r)-1], \quad (1)$$

is shown in Fig. 2 (solid line) together with the experimental curve at 284 K of Bellissent-Funel *et al.*[26] (dotted line). The large differences below $r=1.8$ Å are caused by the intramolecular contributions in the experimental $h(r)$ function (the peak at 1 Å corresponds to the intramolecular OH distance and the peak at 1.6 Å to the intramolecular HH distance). Both curves are in close agreement for $r\geqslant 3$ Å. There are some differences in the intermediate region, which have already been noted by Berendsen *et al.*,[20] which indicate a deficiency of the model.

As a second test of the SPC/E potential, which is more closely related to the simulation of the growth of amorphous ice, we investigate the limit of mechanical stability of SPC/E ice Ih to get a rough estimate for the melting point. The rectangular simulation box for the crystal is built up of 54 units, which contain 8 water molecules each[27] (dimensions of the box: 27.0 Å×23.4 Å×22.0 Å). The water molecules are in such an arrangement that the net dipole moment in each unit is zero. In a constant pressure simulation ($P=0.1$ MPa), the temperature of the system is first increased from 77 to 290 K. From 290 to 310 K the temperature of the external heat bath is increased every 6 ps by 2 K. To detect the melting of the system we monitor five quantities: (i) the total potential energy, (ii) the so-called melting factor,[25] (iii) the mean squared displacement with respect to the lattice positions, (iv) the density of the system and, (v) the actual temperature which is slowly increasing due to the heat bath. In Figs. 3 and 4, the different quantities are displayed for the first- and second-half of the heat bath temperature range. In Fig. 4, we find continuous changes in the monitored quantities. In Fig. 3, these quantities are displayed for the temperature range between 292 and 300 K on finer scales. In these diagrams, we see a slight increase in potential energy of about 1 kJ/mol, an increase of the mobility and a drop in the melting factor after about 6000 time steps, corresponding to a heat bath temperature of 296 K. In view of the fact that the temperature increase is very fast in comparison to experimental heating rates, we conclude, that the thermodynamic melting point of SPC/E water will be lower than this value. For comparison, Weber and Stillinger observed 300 K for the melting temperature of a ST2 model ice cluster,[28] Karim and Haymet from the simulation of the ice/water interface a value of 240 K for TIP4P[27] and of about 200 K for SPC water.[29] For the latter model, which is closely related to our SPC/E model, Ji and Pettitt[30] recently determined the melting point to be at about 260 K. From the general properties of these two related models, we would expect a higher melt-

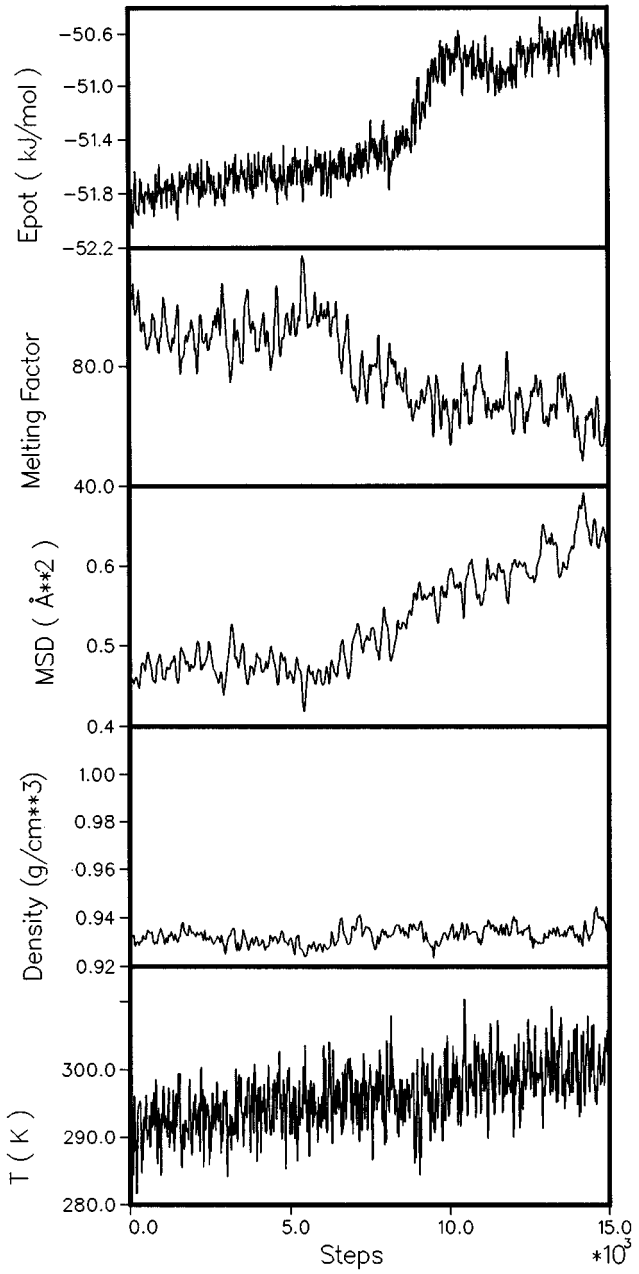

FIG. 3. Melting of ice: Every 3000 steps the temperature of the heat bath is increased by 2 K. From 292 to 300 K.

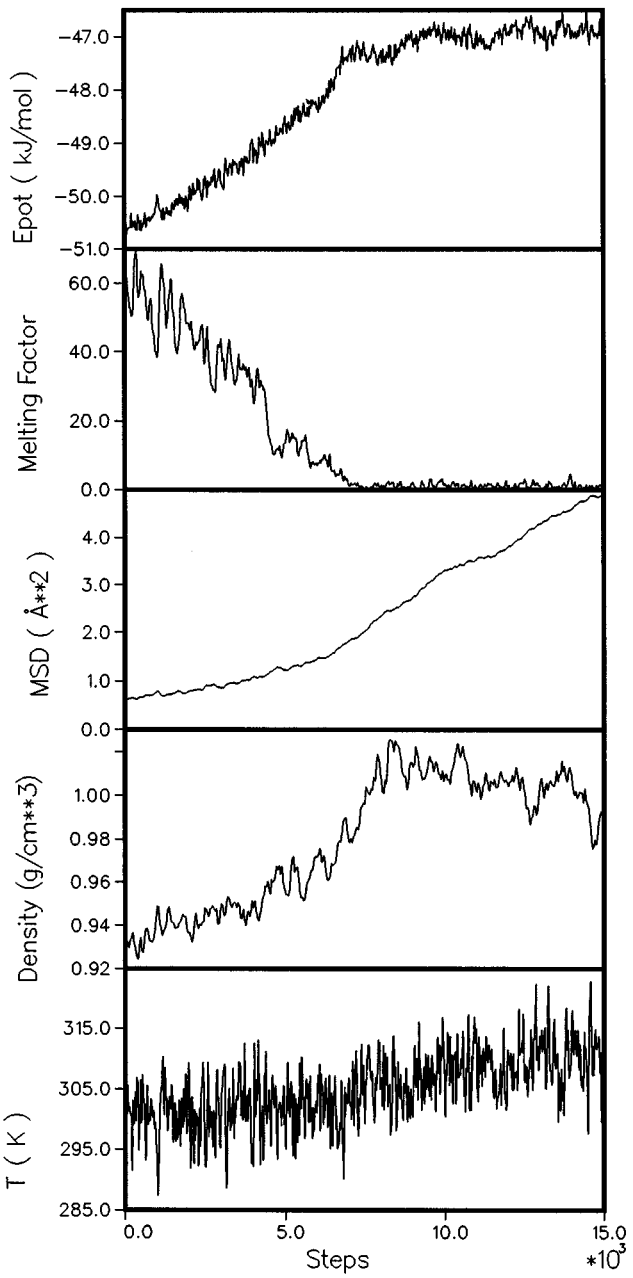

FIG. 4. Melting of ice: Every 3000 steps the temperature of the heat bath is increased by 2 K. From 302 to 310 K.

ing point for SPC/E, in agreement to our observation of the mechanical stability limit.

IV. SURFACE STRUCTURE AND DENSITY OF THE VAPOR DEPOSITED AMORPHOUS ICE LAYER

During the simulation of the vapor deposition we generate an ice layer of 500 water molecules. As a first attempt to characterize this layer, we make a scan of the surface. For this purpose, we define a grid of $(n\times n)$ points in the (x,y) plane. Graphically, at each point of the grid a sphere of radius r_{sp} is lowered from positive z values until the surface of the sphere touches one of the oxygen coordinates of one water molecule. The corresponding coordinate of the center of the sphere is stored as a surface point. With a similar method, it is possible to scan the bottom surface of the ice layer. In Figs. 5 and 6, the upper and lower surface of the ice layer are displayed for a grid of (20×20) points and $r_{sp}=3$ Å. One can clearly see that the upper surface is strongly structured with deep valleys. It indicates that there is no profound restructuring of the surface during the simulation. The pronounced structure of the upper surface corresponds to the experimental fact that the surface area of vapor deposited amorphous ice is very large.[31] On the other hand, the lower surface is rather flat. The flatness of the lower surface indicates the presence of a homogeneous first layer at the substrate.

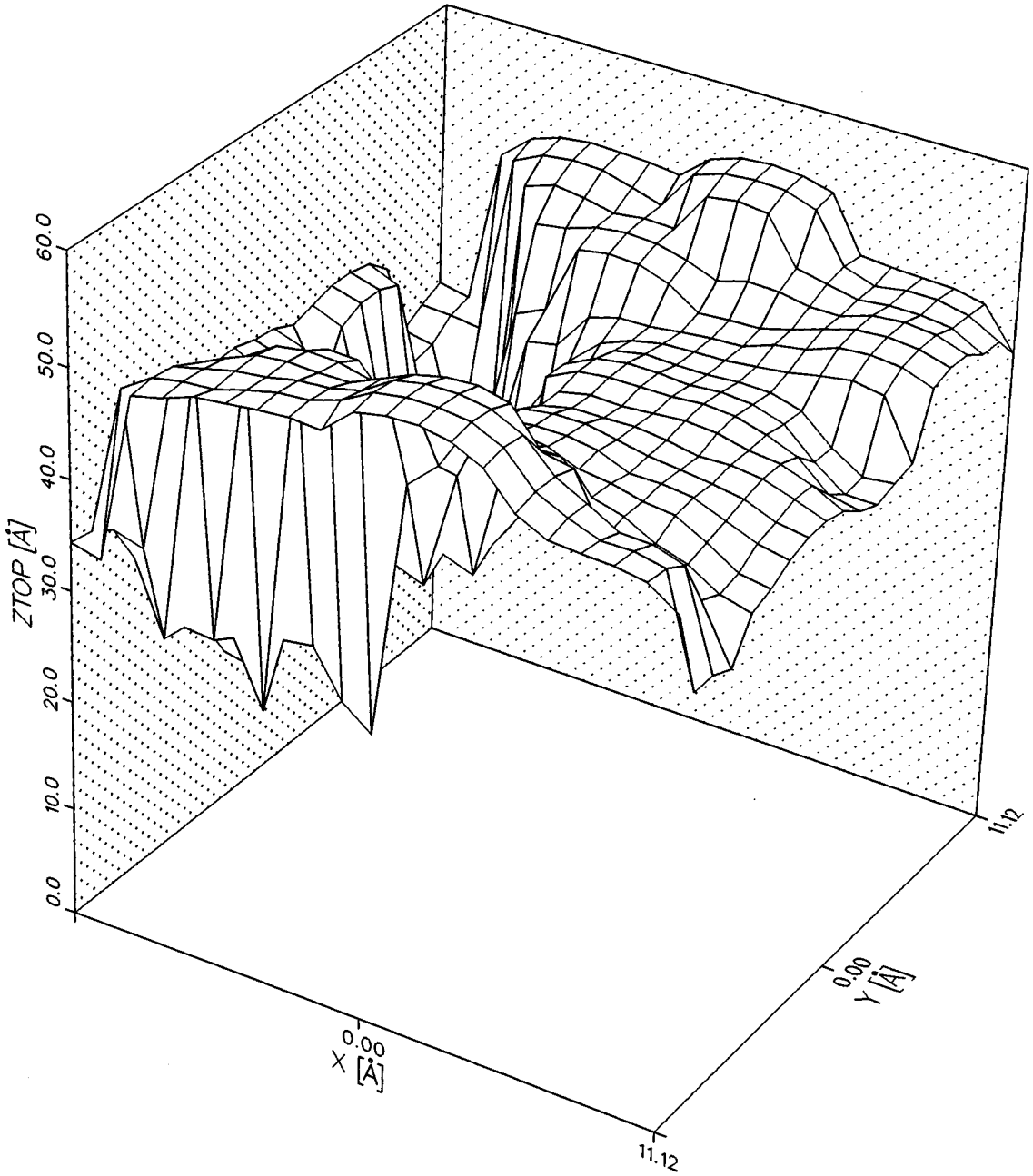

FIG. 5. The upper surface of the vapor deposited amorphous ice layer (note the different scale in z direction).

From the calculation of the upper and lower surface of the ice, it is also possible to calculate the volume of the ice and since the number of molecules is known, the density of the amorphous ice. The problem with this method is the fact that the calculated density is a function of the radius of the scanning sphere. In Fig. 7, the density is drawn as a function of the radius r_{sp} of the sphere. The density increases steadily from 0.75 to 1.1 g/cm^3. Because of the monotonic shape of the curve it is difficult to extract an unambiguous value. One possible choice for r_{sp} would be the intermolecular OH distance of 1.74 Å giving a density of about 0.93 g/cm^3. Choosing r_{sp} to be 1.37 Å (half of the OO distance) leads to a density of 1.08 g/cm^3.

That these values are reasonable, can be seen from the distribution of the height z of the water molecules from the surface. In Fig. 8, the local density of the oxygen atoms is plotted vs height z. The substrate layers are not displayed in Fig. 8. At low z values, there is a sharp peak around 6 Å. This peak reflects the existence of an adsorbate layer. The adsorbate layer causes the very flat lower surface of the ice layer (Fig. 6). The second layer at 8 Å is much less pronounced and at higher z values we find no further structure. At z values greater than 20 Å, the mean density decreases. In this region, the density is lowered by the deep valleys which can be seen in the picture of the upper surface of the ice layer (Fig. 5). If we calculate the average density for a layer ranging from 7.5 to 20 Å, we find a value of 0.94 g/cm^3. Extending the averaging up to 25 Å leads to a density of 0.83 g/cm^3.

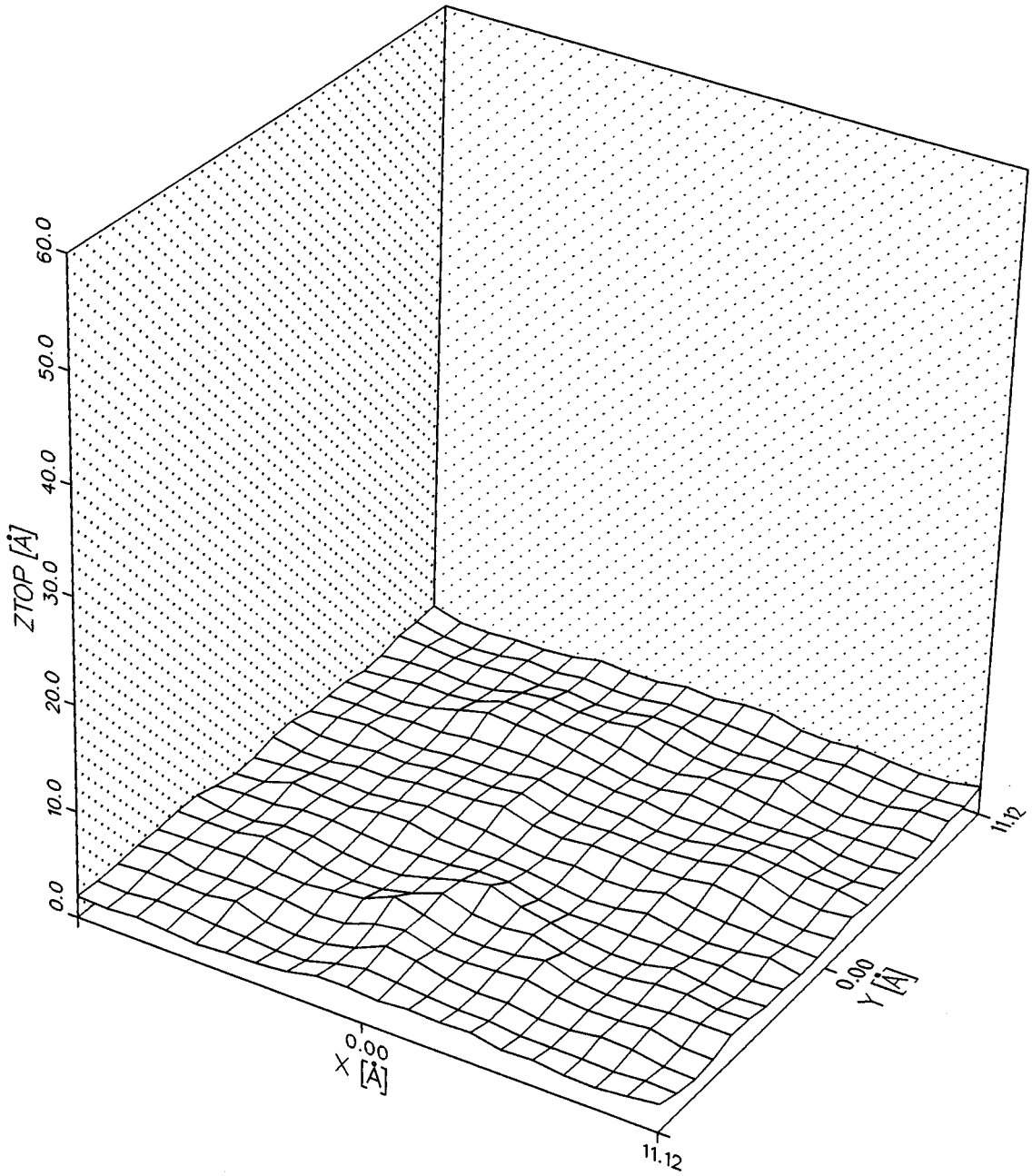

FIG. 6. The lower surface of the vapor deposited amorphous ice layer.

(For the upper part of the ice layer between 20 and 44 Å, we find a density of 0.55 g/cm^3.) Even though the precise values of the density calculated with the two methods are uncertain, they suggest a value in the range of the reported experimental values of 0.94 g/cm^3 (Refs. 16 and 32) and 0.909 g/cm^3 (Ref. 31) for vapor deposited amorphous ice.

V. THE PAIR CORRELATION FUNCTIONS

To compare the structure with experimental data, we first calculate the partial pair correlation functions. In view of the surface roughness, we consider for this only molecules within the slab from $z=5.8$ to 24.8 Å.

For the calculation of the radial pair correlation function the actual number of neighbors in the spherical shell between r and $r+dr$ around a given particle has to be divided by the corresponding number of neighbors dN in a reference system of homogeneous density ρ_0. If we denote the volume of this shell by dV we obtain: $dN=\rho_0 dV$. Since we regard only particles in the slab between 5.8 Å$\leqslant z \leqslant$24.8 Å we have to use formulas for segments of spherical shells. The volume element becomes therefore a function of the radius r and the position z of the reference molecule within the slab: $dV=dV(r,z)$. The appropriate formulas are elementary, but lengthy, due to the discrimination between different geometric cases. Since the reference water molecule for the calcu-

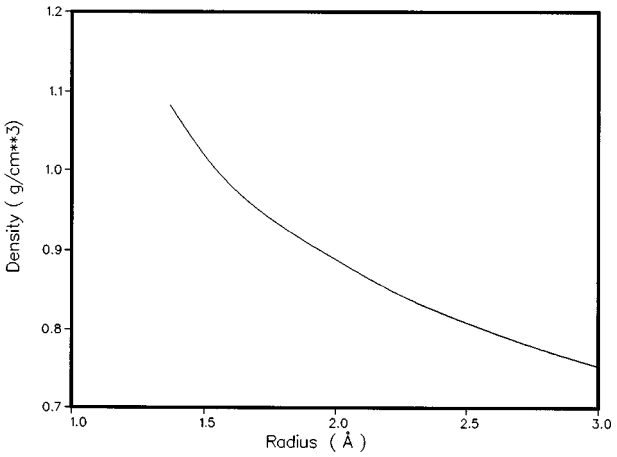

FIG. 7. The density of the ice as a function of the scanning sphere (see the text).

lation of the pair distribution function can be at any height z within the system we have to average out the z dependence by integrating over all possible z values. This implies the assumption of a homogeneous distribution of molecules within the slab. After averaging we obtain an expression for the volume element dV between a given r and $r+dr$.

Dividing the average number of molecules found during the simulation in the slab by its volume, gives the density of the homogeneous reference system. For the above mentioned choice of the slab of thickness $d=19.0$ Å we find $\rho_0=0.96$ g/cm^3. The pair correlation function was calculated with a resolution of $dr=0.043$ Å. As seen from Fig. 9, nevertheless the pair correlation functions are slightly dropping. This is probably due to inhomogeneities within the slab.

In Fig. 9, the three different partial pair correlation functions g_{OO}, g_{OH}, and g_{HH} are displayed (solid line). In comparison with the pair correlation functions of liquid water, these functions are very sharply peaked. For example, in the liquid state of the SPC/E model, the height of the first maximum of g_{OO} is only about three[20] instead of more than eight

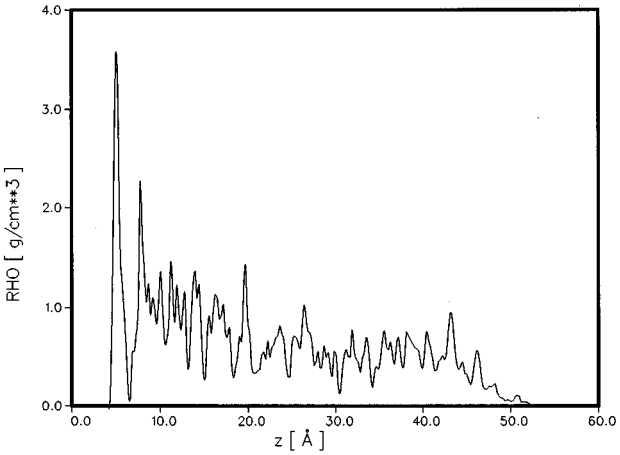

FIG. 8. Local density as a function of the height z.

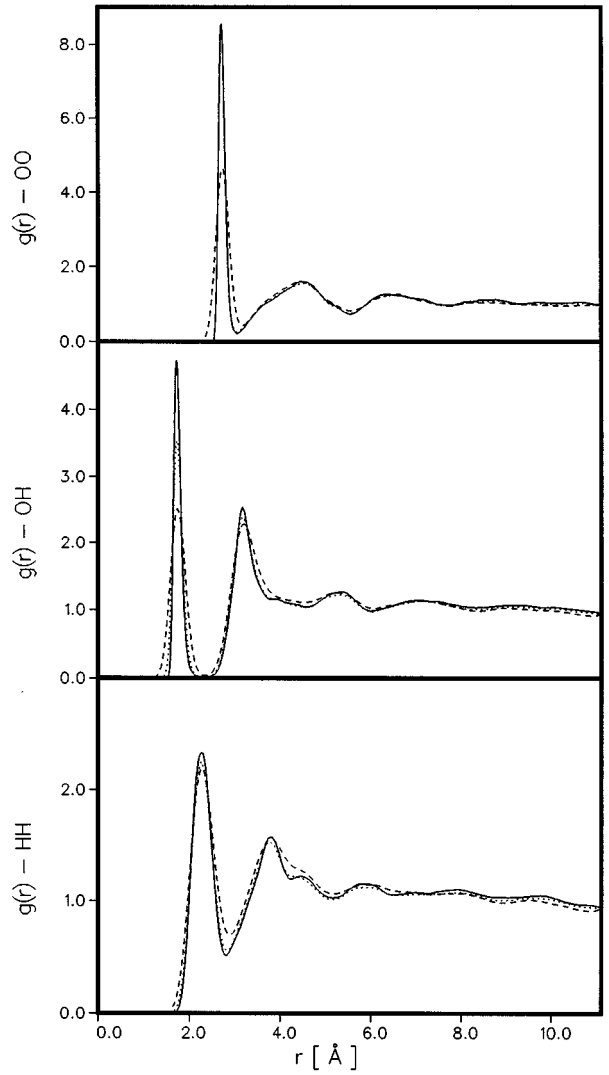

FIG. 9. Pair correlation functions of the vapor deposited amorphous ice. Solid line: without any corrections. Dotted line: including corrections due to vibrations. Dashed line: including corrections due to vibrations and limited resolution of experiments.

in the present simulation of the amorphous phase. The question arises as to whether these sharp peaks are observable in experiments.

In fact, two modifying influences have to be considered before a comparison with experimental data can be performed. Changes arise from the presence of intramolecular vibrations. In the simulation, any intramolecular degree of freedom is neglected, because in the SPC/E model the water molecule is treated as a rigid body. To investigate the influence of intramolecular vibrations, we choose the method of Kuharski and Rossky.[33] For the calculation of the pair correlation functions, the coordinates of the classical simulation are replaced by coordinates with modified r_{OH} distances and modified $\angle$(HOH) angles. The deviations of the r_{OH} distances and the $\angle$(HOH) angles from their equilibrium values are chosen according to a Gaussian distribution with a root mean square variation in the angles of 8.72° and in the bond length of 0.0677 Å.[34] It should be emphasized that the molecular dynamics simulation is not influenced by this replace-

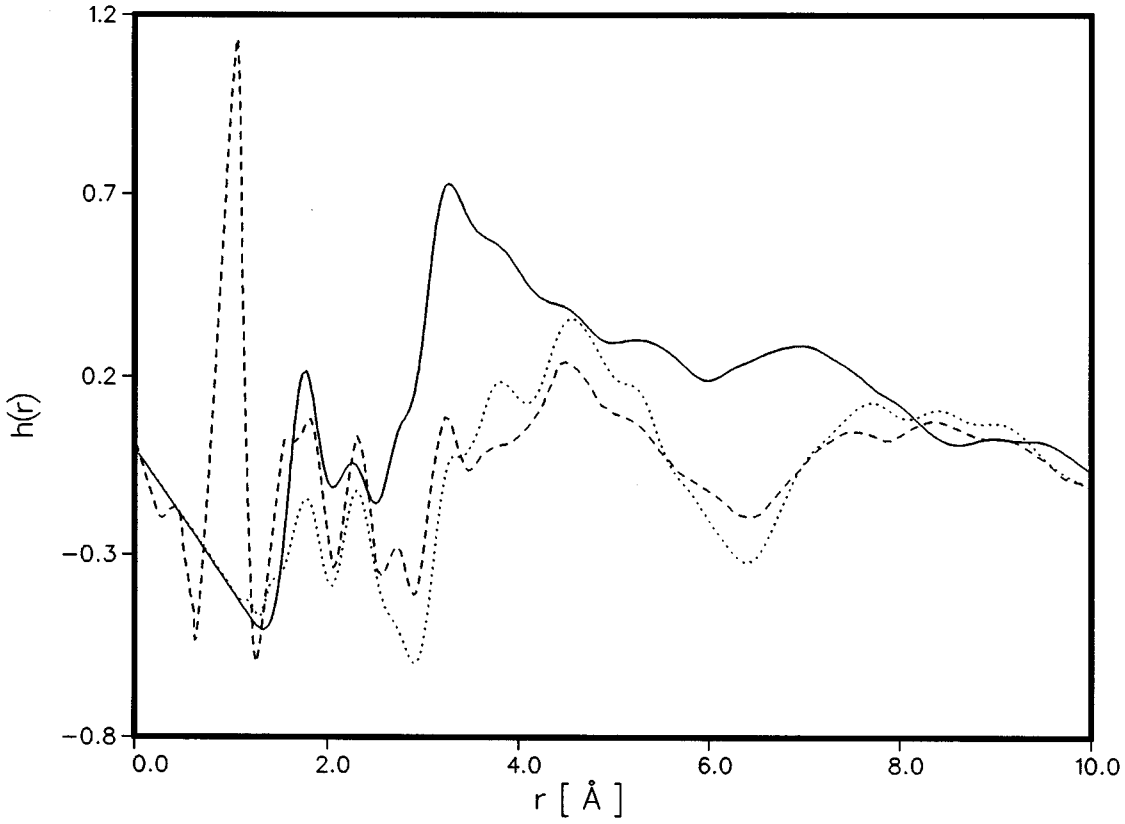

FIG. 10. $h(r)$ function of the amorphous ice. Solid line: simulation. Dotted line: vapor deposited ice [Chowdhury *et al.* (Ref. 18)]. Dashed line: lda ice [Bellissent-Funel *et al.* (Ref. 26)].

ment, as this is only done during the data analysis. In Fig. 9, the resulting $g(r)$ functions are shown as dotted lines. The g_{OO} function is almost not effected at all because the oxygen atoms are much heavier than the hydrogen atoms. The strongest influence can be seen in the first peak of the g_{OH} function. The height of the first peak decreases from 4.8 to 3.5. The influence on the g_{HH} function is weaker because the peaks are initially much broader.

Additionally, the experimentally determined $g(r)$'s are influenced by the limited resolution of the neutron scattering experiments. According to Chowdhury *et al.*,[18] the limited range of q values leads to a broadening of the lines with a full width at half maximum (FWHM) of

$$\Delta r \simeq \frac{5.44}{q_{\max}}. \tag{2}$$

Chowdhury *et al.*[18] measured up to a maximum q value of $q_{\max}=19$ Å^{-1}, leading to a FWHM of 0.29 Å. Convoluting the $g(r)$ functions with a Gaussian having a FWHM of this value leads to the dashed lines of Fig. 9. There are remarkable changes in all three $g(r)$ functions. The first peak in g_{OO} reduces from 8.6 to 4.7. The first peak in the g_{OH} reduces from 3.5 to 2.6. The changes in the g_{HH} functions are less pronounced.

A. Comparison with experimental $h(r)$ functions

To compare the simulated structure with experiments, we calculate the $h(r)$ function of Eq. (1), using the corrected (dashed) pair correlation functions of Fig. 9. In Fig. 10, $h(r)$ is plotted together with the experimental curves of Chowdhury *et al.*[18] and Bellissent-Funel *et al.*[26] Chowdhury *et al.*[18] produced the amorphous ice by vapor deposition, while Bellissent-Funel *et al.*[26] made the amorphous ice via the pressure melting of hexagonal ice Ih. Despite the differences in the production, both curves are similar and ascribed to a lda ice form. The differences in these curves for r values lower than 1.8 Å are again caused by the fact that in the curve of Chowdhury *et al.*[18] only intermolecular contributions are shown, while in the curve of Bellissent-Funel *et al.*,[26] intramolecular contributions are also present. For r values greater than 3 Å both curves show a broad structured maximum at 4.5 Å, a minimum at 6.5 Å and a flat maximum around 8.5 Å.

The features of the simulated curve differ appreciably from the features of these experimental curves: in the simulated curve, we find a maximum at 3.3 Å, a minimum close to 6 Å, and a maximum at 7 Å. In general, the extrema are shifted to lower r values. Also, the shapes of the maxima at 3.3 and 4.5 Å are different. [Due to the problems in the normalization of the $g(r)$'s, which are amplified in the $h(r)$ function, the simulated $h(r)$ function decreases at larger r values.]

In view of these large discrepancies, it is very interesting to compare the simulated curve with the experimentally determined $h(r)$ function of hda ice[26] (Fig. 11). This shows that the shapes of the simulated curve and of the experimen-

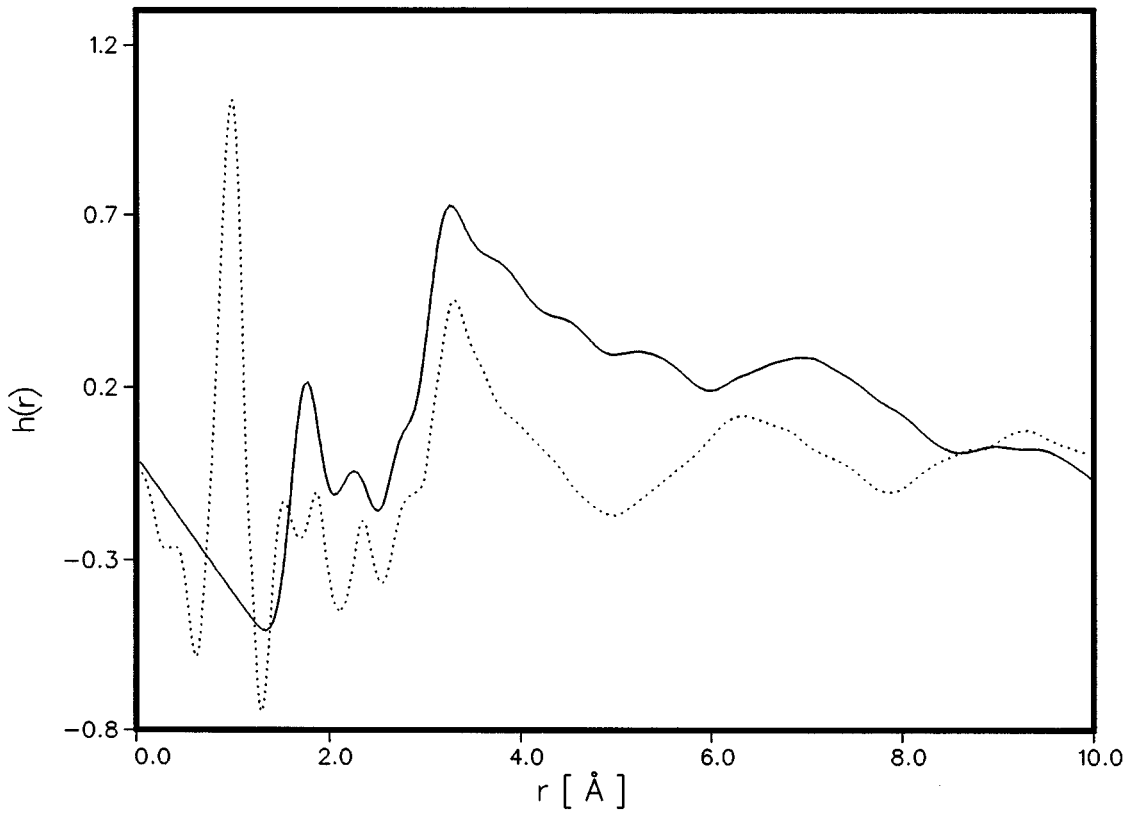

FIG. 11. $h(r)$ function of the amorphous ice. Solid line: simulation. Dotted line: high density ice [Bellissent-Funel *et al.* (Ref. 26)].

tal hda curve are more similar. The positions of the peaks at 3.3 Å are identical. The positions of the following minima and maxima are shifted to lower r values in the hda curve. In contrast to this, Fig. 10 shows that the positions of the peaks of the experimental curve for lda ice are shifted to higher r values. Accordingly, the $h(r)$ function of the simulated ice can be categorized as being in between both experimental curves, but closer to hda ice. In fact, a linear combination of the hda and lda curves of Bellissent-Funel *et al.*[26] (reproduced in Figs. 10 and 11), shows closest resemblance to the simulated $h(r)$ function, when weighted with factors 0.7 and 0.3, respectively.

Recently, Davies and Dore performed new measurements on vapor deposited amorphous ice.[35] In Fig. 12, their $h(r)$ curve is shown in comparison to the simulated curve. Considering the appreciable normalization problems due to the geometry and roughness of the amorphous ice layer (as described above), there is a reasonable agreement between these two distribution functions with respect to the shape of the curves and the positions of the maxima and minima. At the moment, it is not known which differences in the experimental setup cause the differences to the experimental curves of Chowdhury *et al.*[18] It is, however, well known that a variety of parameters can influence the deposition of amorphous ice,[1] moreover, the recent experiments of Jenniskens and Blake[5] suggest the existence of a smooth transition between a high and a low density form of vapor deposited amorphous ice. This transition region could well be crossed in the course of a deposition experiment due to energy removal problems, such as large layer thickness or high deposition rates.

B. Comparison with amorphous ice cluster simulations

Recently, Zhang and Buch reported simulations of the growth of amorphous clusters in the gas phase[12–14] (In the following, we only refer to simulation "C" of their study, where the TIPS2 interaction had been used.). They report a density of 1.36 g/cm^3 for a cluster with 168 molecules and of 1.32 g/cm^3 for the same cluster after having grown to 296 molecules. These values are clearly higher than the value found in this study and the experimental values.[16,31,32] It is possible that they are influenced by difficulties in the proper determination of the effective volume in this geometry.

Because of the resulting difficulties in the normalization of the $g(r)$'s in the simulations of Zhang and Buch,[12–14] we compare in Fig. 13 the weighted sum

$$g_{\mathrm{tot}} = 0.092 \cdot g_{\mathrm{OO}} + 0.422 \cdot g_{\mathrm{OH}} + 0.486 g_{\mathrm{HH}} \tag{3}$$

of the $g(r)$'s of the simulation of Zhang and Buch[13] with the sum of the partials from our deposition simulation (Fig. 9). The positions of the peaks are the same, while the height of the peaks and their ratios are different. Differences are not only due to the normalization but may also be produced by different resolution in the calculation of the $g(r)$'s. Taking this into account, the two simulation studies yield rather similar structures.

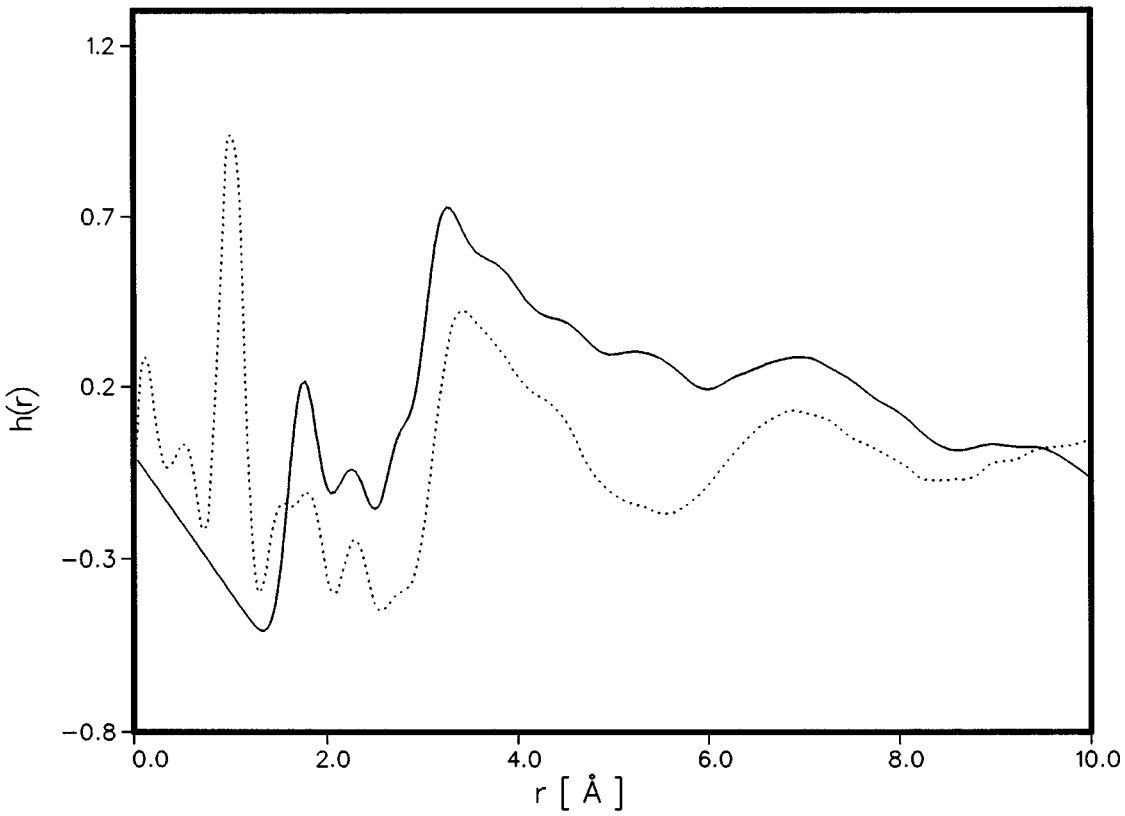

FIG. 12. $h(r)$ function of the amorphous ice. Solid line: simulation. Dotted line: vapor deposited ice [Davies and Dore (Ref. 35)]. Note that in the experimental curve inter- as well as intramolecular correlations contribute to the overall scattering data. However intramolecular peaks are confined to distances smaller than 1.7 Å. The decrease of the simulated $h(r)$ at large r values is due to the problems with the normalization of the $g(r)$'s, as explained in the text.

C. Comparison with quenched amorphous ice

For completeness, we make a comparison with simulated amorphous ice formed by *rapid cooling* of liquid water to 77 K. Two different temperature profiles are used for the production of the quenched amorphous ice. In the first run, the temperature is lowered exponentially:

$$T=300\ \exp(-\alpha t)\ \ \mathrm{K} \tag{4}$$

with $\alpha=1.36\times10^{10}\ \mathrm{s}^{-1}$.

Within 100 ps, a temperature of 77 K is reached. However, the temperature regime with high mobility is passed very quickly. After 13.4 ps a temperature of 250 K, where the system loses mobility, is reached. Therefore, a second profile is used. In this profile, the temperature is lowered linearly within 80 ps from 300 to 200 K and then linearly within the next 20 ps to 77 K. The first run is referred to as the fast quench and the second as the slow quench. During both quenching processes we observe no significant density change. The $g(r)$'s of both runs are displayed in Fig. 14. Differences between the $g(r)$'s resulting from the different quenching schemes are hardly to be seen (note that these curves are not corrected). In Fig. 15, the corresponding $h(r)$'s of the two runs are shown together with the experimental lda ice curve of Chowdhury *et al.*[18] Now we can clearly observe a difference between the two simulation runs, which can be characterized as a small but systematic approach to the lda ice structure of Chowdhury *et al.*,[18] when passing from the fast to the slow quench.

A similar behavior had been observed in a previous study of stretched water using the ST2 potential.[36] There it was shown that these changes are indicative for the formation of a more perfect tetrahedral hydrogen-bond network.

The slightly different slopes in the linear region of $h(r)$ at small r values result from the different densities used for the evaluation of the experimental compared to the simulation data.

VI. CHARACTERIZATION OF THE HYDROGEN-BOND NETWORK

It is well known that liquid water is a globally connected random and essentially tetrahedral hydrogen-bond network.[36–39] Therefore, the question of the network structure in the amorphous state arises. The definition of a hydrogen bond is not unambiguous. In simulation studies, geometric and energetic criteria are used. We call a pair of water molecules hydrogen bonded if the (OO) distance is lower than 3.4 Å (corresponding to the first minimum in the g_{OO} function) *and* the pair interaction energy is lower than -12 kJ/mol. Similar definitions of hydrogen bonds are widely used.[37,40,41] Alternatively, the definition can also be based on the intermolecular (OH) distance.[14]

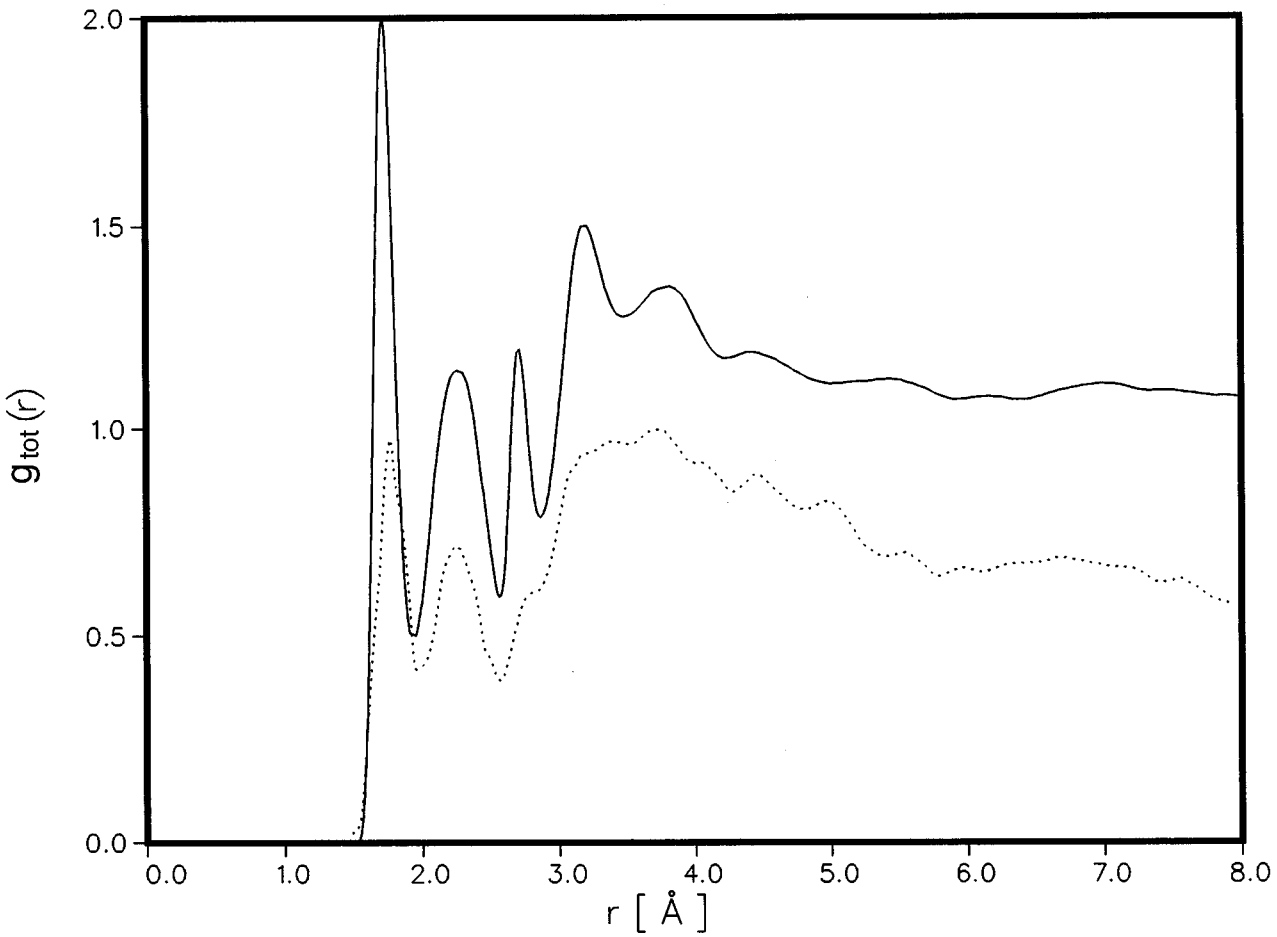

FIG. 13. g_{tot} functions of the simulation of Zhang and Buch (Ref. 13) (dotted line) and the present simulation (solid line).

The number of nearest neighbors n_n (number of molecules within a distance of 3.4 Å) is given in Table I. In agreement with the global densities, the number of neighbors in the liquid phase is highest, while the quenched ice and the vapor deposited amorphous ice have considerably fewer neighbors. In Fig. 16, the distribution of interaction energies for pairs, which meet the above distance criterion is shown. It can be seen that the distributions are narrower in the amorphous phase than in the liquid state. Comparing the different amorphous ices, a further shift to the absolute pair energy minimum of the model (−30 kJ/mol) is seen in the vapor deposited structure, indicating the presence of even more of the strongest hydrogen bonds.

By application of the given geometric–energetic criterion, the number of hydrogen bonds per molecule can be calculated. In Table II, the percentage of molecules with n hydrogen-bonded neighbors is listed together with the average number of hydrogen bonds per molecule. It is satisfying to see that even though in the study of Buch[14] the simulation conditions were quite different and the hydrogen bond definition was based on the intermolecular (OH) distance, the resulting coordination numbers are rather similar. However for the 2 and 5 coordinated molecules fractions of 7% and 6% were obtained. These differences could be a result of the differences in the simulation conditions, however, since the absolute numbers are small we expect them to be not significant. The distribution for the liquid is very broad with a large number of twofold and threefold bonded molecules. The distribution in the fast quench is much narrower and is narrowest in the slower quenched structure. This is in agreement with the structural changes, discussed in connection with Fig. 15. The vapor deposited amorphous ice shows a significantly higher amount of threefold bonded molecules. This is certainly due to the presence of the deeply fissured surface. In contrast to the number of neighbors n_n, the average number of hydrogen bonds per molecule n_{HB} is lowest for liquid water and highest for the amorphous solid resulting from the slow quench. The value for the vapor deposited ice is intermediate. This shows that many of the neighbor molecules in liquid water are in energetically unfavorable positions or orientations. In the amorphous ice, the structure of the hydrogen-bond network is better developed, leading to a decrease of the local density and an increase of the number of hydrogen-bonded neighbors. The smaller number of hydrogen bonds in the vapor deposited amorphous ice contrasts with the shift of the pair energy distribution of Fig. 16, which indicates an increased number of *strong* interactions. This may be explained by the high porosity of the vapor deposited ice. A reliable separation of other influences, like system size and boundaries, may be obtained by more extended simulations.

To get a more detailed description of the existing local

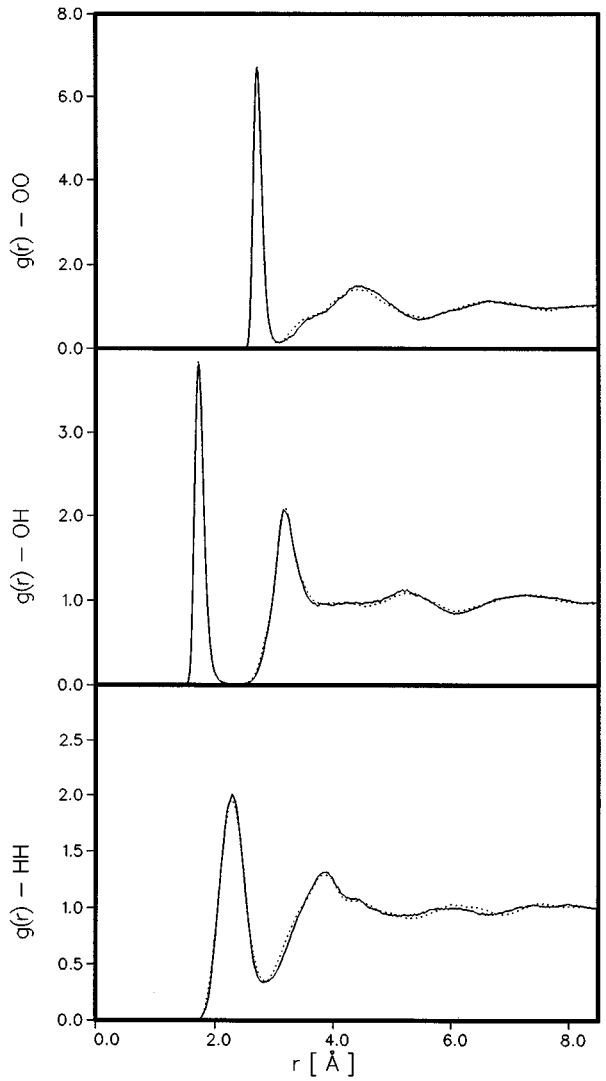

FIG. 14. Pair correlation functions of the fast quench (dotted line) and slow quench (solid line).

molecular arrangements, we apply a procedure of Stillinger and Rahman,[42] which distinguishes between nearest neighbors on positions favorable for hydrogen bonding (''tetrahedral positions *t*'') and others (''interstitial positions *i*''). To this end an octahedron is centered at each oxygen nucleus and oriented so that the four tetrahedral directions emanating from that nucleus which could form undistorted hydrogen bonds, simultaneously pass through the centroids of four, now adjacent faces [see Fig. 6(b) of Ref. 42]. Nearest neighbors ''seen'' from the central oxygen through such faces we call *t* neighbors, the others, *i* neighbors. In low density crystalline ice, only *t* neighbors would be found, while in high density ice crystals with interpenetrating hydrogen-bond networks *i* neighbors would also be found. Table I gives the number of *t* and *i* neighbors n_t and n_i, as well as the number of *t* neighbors, which are hydrogen bonded to the central molecule n_t^{HB}.

Comparison of the slowly quenched and the vapor deposited ice shows a stronger distortion of the latter. Although in both cases practically the same number of neighbors n_n is found, they are in less favorable positions. This can be explained by the geometrical restrictions on the surface or in the vicinity of large pores. As the ratio n_t^{HB}/n_t shows, in all three solid amorphous states only about 5% of the molecules which are in the favorable *t* positions are not bonded (orientationally disordered), whereas in the liquid there are 22%. The difference between vapor deposited and quenched amorphous ice is mainly due to the number of neighbors in interstitial positions. Thus a slightly closer resemblance to the local order in high density crystalline ice is found in the vapor deposited form. The presence of ''interstitial water'' has also been suggested to be an important structural feature of a high density form of amorphous ice, obtained by Narten *et al.*[16]

Due to the construction principles of the so-called continuous random network model (CRN), which has been used to describe the structure of lda ice,[1,18] no *i* neighbors would be expected in this model. Therefore, the number n_i can be considered as a measure of the deviation from the CRN model. In contrast to the vapor deposited ice of Chowdhury *et al.*,[18] the present structures show strong deviations from CRN.

The distribution of the angles formed by triples of hydrogen bonded molecules (to be more precise, the angle formed by the vectors which connect a central molecule with two hydrogen-bonded neighbors) gives further insight into the structure of the network. In Fig. 17, the distribution of these bond angles is shown for the four systems. In all simulations, the mean bond angle is very close to the ideal tetrahedral angle of 109°. The width of the distribution for the four systems is different, however. The rms deviation for liquid water is 24°, for the amorphous solid from the fast quench 20°, for the amorphous solid from the slow quench 19°, and for the vapor deposited ice 22°. Again, the slowly quenched amorphous ice shows the narrowest distribution, indicating the highest order. The distribution of the vapor deposited ice is significantly disturbed due to its porosity. All of these values are much larger than the variance of 8° estimated from x-ray diffraction data.[16] This observation is in accord with the previous observation of Zhang and Buch.[13]

To summarize the results of the hydrogen-bond analysis, it can be stated that the network of the amorphous ice is better ordered than that of liquid water. The slowly quenched amorphous ice seems to have the best ordered structure, while the vapor deposited ice is significantly more disturbed.

VII. DISCUSSION

We studied the formation of amorphous ice by vapor deposition in computer simulations. The results of the present simulation are comparable to the $h(r)$ function of a recent neutron scattering experiment of Davies and Dore[35] (Fig. 12) as well as the results of Zhang and Buch[12–14] which simulated the growth of amorphous ice clusters in the gas phase (Fig. 13).

Comparing our results with the neutron scattering results for hda and lda ice, which had been produced by the transformation of crystalline ice via application of pressure, our vapor deposited ice shows an intermediate structure, although closer to hda than to lda ice. [Here it is interesting to

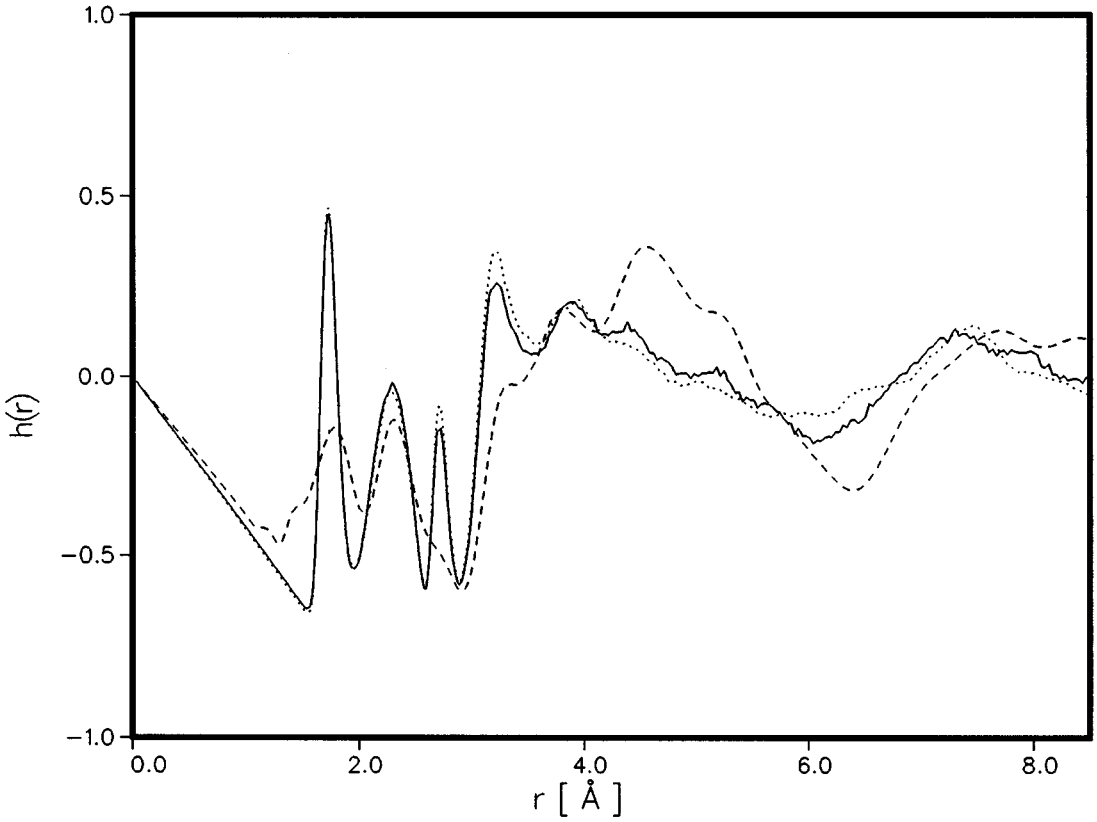

FIG. 15. $h(r)$ function of the fast quench (dotted line) and slow quench (solid line) compared to vapor deposited ice of Chowdhury *et al.* (Ref. 18) (dashed line).

note that $h(r)$ of liquid water is also closer to hda than to lda (compare, e.g., Fig. 2 with Figs. 10 and 11).] The structural differences appear in shifts of the positions of the maxima and minima in the $h(r)$ functions. These shifts to larger r values, when passing from hda to our vapor deposited ice and then to lda ice, corresponds to shifts of the first peak of the static structure factor $S(Q)$ to smaller Q values, and indicate an increasing long range order. A similar shift has been observed when lowering the temperature in supercooled water[43] and was interpreted along the same lines. The similarity of the structure obtained in the present simulation with hda structure and the liquid structure suggests that the formation of the observed amorphous ice structure is due to the strong coupling of the amorphous ice to a heat bath that takes out the thermal motion of the water molecules very quickly. The fast cooling of the arriving molecules prevents the water molecules from optimizing their local geometrical arrangement towards a more perfect four bonded network. The time scale of the simulation is apparently not large enough to allow the ''healing'' of the hydrogen bonded network which gives rise to long range correlations as seen in experiments.[18] In the recent electron diffraction study of vapor deposited amorphous ice by Jenniskens and Blake,[5] the temperature dependence of the position of the first diffraction maximum has been interpreted as being indicative of a structural transition from high density amorphous ice, produced by vapor deposition at 15 K, to a lower density form above 70 K. This suggests that the high density form of vapor deposited amorphous ice is not a sporadically occurring artifact, but rather a reproducibly formable structure with a specific range of metastability. Obviously, comparable structures have now been observed several times experimentally (Narten *et al.*,[16] Davies and Dore,[35] and Jenniskens and Blake)[5] and have been produced by computer simulations (Ref. 13 and this work).

TABLE I. Number of neighbors in favorable and unfavorable hydrogen-bonding positions (see the text).

	n_t	n_t^{HB}	n_i	$n_n=n_i+n_t$	$\frac{n_t^{\mathrm{HB}}}{n_t}$
Liquid water	3.48	2.73	1.28	4.76	0.78
Fast quench	3.77	3.54	0.70	4.47	0.94
Slow quench	3.77	3.60	0.55	4.32	0.95
Vap. deposition	3.54	3.37	0.83	4.37	0.95

Comparing the different amorphous ices produced in this simulation study, various distribution functions also suggest a strong influence of the porosity on the structure of the vapor deposited ice, compared to the amorphous ice produced by quenches from the liquid. This conforms with the observation of the deeply fissured surface, shown in Fig. 5.

In summary, there seems to be now some evidence from experiments and simulations that it is possible to get a high density form of amorphous ice in vapor deposition experiments. Moreover, a broad transition region between these

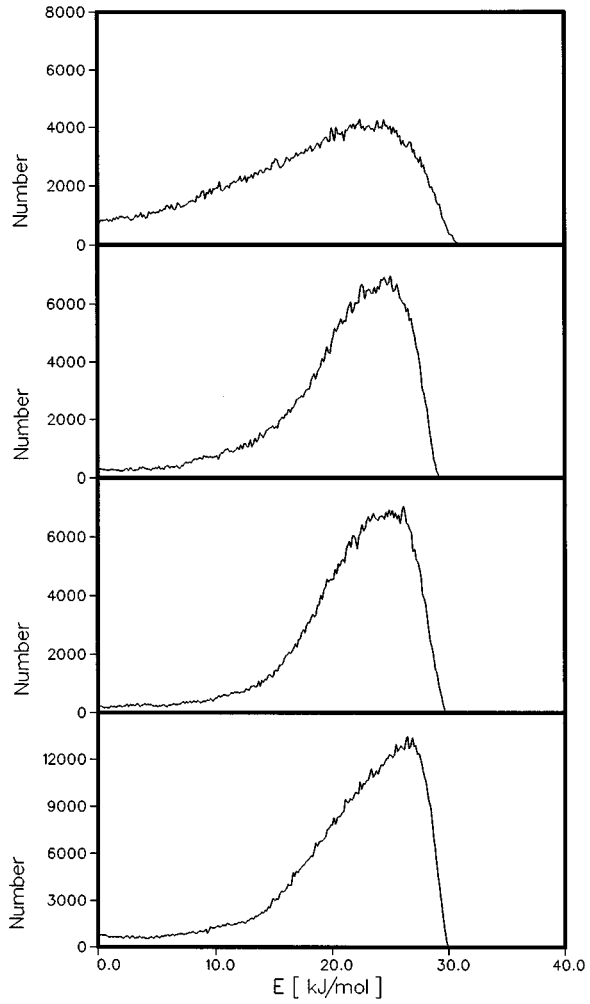

FIG. 16. Number of nearest neighbor pairs with interaction energies E for liquid water at 306 K (top), for the fast quench (second), slow quench (third), and vapor deposited (bottom).

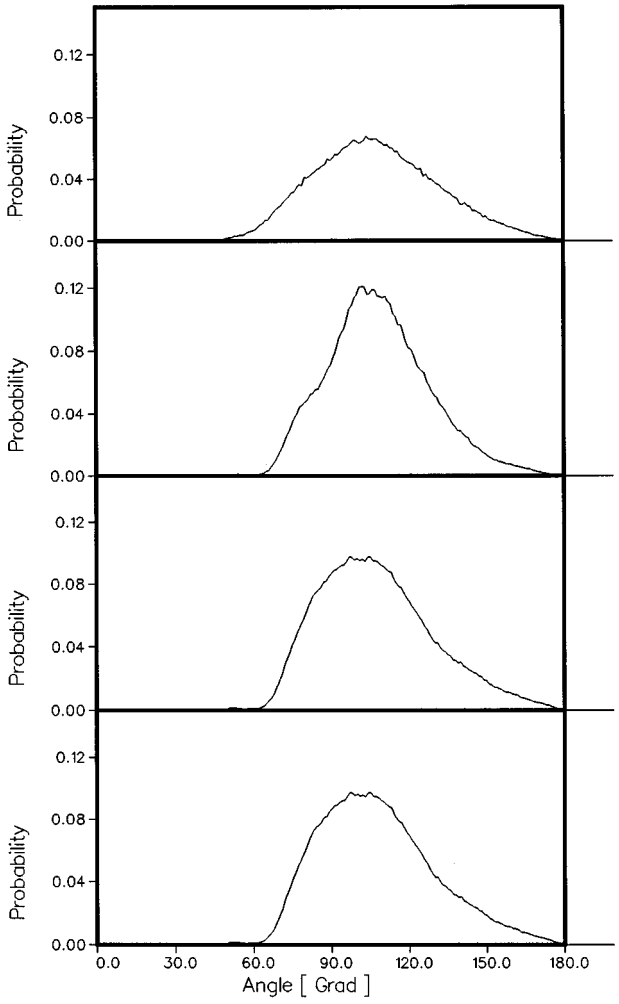

FIG. 17. Distribution of (OOO) angles for liquid water at 306 K (top), for the fast quench (second), slow quench (third), and vapor deposited (bottom).

two possible forms between about 35 and 70 K (Jenniskens and Blake)[5] also allows the occurrence of intermediate structures, depending on the experimental conditions. In this regard, our simulations yielded a structure in the transition region, although, due to the imperfections of the potential model and the simulation procedure, the picture is not unambiguous. The microscopic structure represented by the pair distribution functions, is closer to high density amorphous ice, even though the average density, which is hard to determine seems to be closer to lda ice. From the conditions, under which the deposition has been carried out in the simulation runs, the occurrence of an intermediate structure is reasonable, as the surface temperature had been set to 60 K. The action of the necessary heat bath probably shifted the ''effective surface temperature'' to an even lower value by limiting the local heating and therefore the restructuring of the hydrogen bond network.

TABLE II. Percentage of molecules with n hydrogen bonds and the mean value of the hydrogen bonds n_{HB}.

Number of HB	1	2	3	4	5	6	n_{HB}
Liquid water	2.6	16.5	40.5	37.2	3.2	0.0	3.22
Fast quench	0.0	1.8	15.9	79.8	2.5	0.0	3.83
Slow quench	0.0	0.6	12.7	83.7	3.0	0.0	3.89
Vap. deposition	0.0	3.4	21.2	72.2	3.1	0.0	3.75

Since the preparation of this manuscript, we have received further information on more recent neutron measurements of amorphous ice. The work of Blakey and Dore[44] has shown that the low-density amorphous ice is well represented by a continuous random network (CRN) and is almost identical to the structure of hyperquenched solid water. However, the results also cast some doubts on the work of Davies *et al.*[35] suggesting that there may be some nitrogen contamination in the sample. These imply that the ''intermediate density'' form could be an artifact in which the enclosed nitrogen atoms act as apolar molecules and disrupt the open tetrahedral network of the pure amorphous ice. In view of this fact, there now appears to be two possible explanations for the experimental results: the nitrogen contamination as well as very low deposition temperatures, form a barrier to the formation of a fully connected network of tetrahedral H bonds which has been observed in low density amorphous ice.

ACKNOWLEDGMENTS

We would like to thank P. H. Poole, F. Sciortino, and F. H. Stillinger for valuable discussions, E. Davies and J. Dore, also, for communication of their neutron scattering results prior to publication, the Höchstleistungsrechenzentrum (HLRZ) Jülich for a generous amount of computer time and the Fonds der Chemischen Industrie for financial support.

[1] M. G. Sceats and S. A. Rice, in *Water, A Comprehensive Treatise*, edited by F. Franks (Plenum, New York, 1982), Vol. 7, Chap. 2.
[2] P. Mehl and P. Boutron, J. Phys. **48**, C1 449 (1987).
[3] E. Mayer and R. Pletzer, Nature **319**, 298 (1986).
[4] N. J. Sack and R. A. Baragiola, Phys. Rev. B **48**, 9973 (1993).
[5] P. Jenniskens and D. F. Blake, Science **265**, 753 (1994).
[6] E. Mayer and P. Brüggeller, Nature **298**, 715 (1982).
[7] E. Mayer, J. Appl. Phys. **58**, 663 (1985).
[8] J. Dubochet and A. W. McDowall, J. Microsc. **124**, RP3 (1981).
[9] O. Mishima, L. D. Calvert, and E. Whalley, Nature **310**, 393 (1984); **314**, 76 (1985).
[10] P. H. Poole, F. Sciortino, U. Essmann, and H. E. Stanley, Nature **360**, 324 (1992); Phys. Rev. E **48**, 4605 (1993).
[11] J. S. Tse and M. L. Klein, Phys. Rev. Lett. **58**, 1672 (1987).
[12] Q. Zhang and V. Buch, J. Chem. Phys. **92**, 1512 (1990).
[13] Q. Zhang and V. Buch, J. Chem. Phys. **92**, 5004 (1990).
[14] V. Buch, J. Chem. Phys. **96**, 3814 (1992).
[15] M. A. Wilson, A. Pohorille, P. Jenniskens, and D. Blake, Orig. Life Evol. Biosph. (1995) (to be published).
[16] A. H. Narten, C. G. Venkatesh, and S. A. Rice, J. Chem. Phys. **64**, 1106 (1976).
[17] E. Mayer and R. Pletzer, J. Chem. Phys. **80**, 2939 (1984).
[18] M. R. Chowdhury, J. C. Dore, and J. T. Wenzel, J. Non-Cryst. Solids **53**, 247 (1982).
[19] F. Vesely, *Computerexperimente an Flüssigkeitsmodellen* (Physik, Weinheim, 1978).
[20] H. J. C. Berendsen, J. R. Grigera, and T. P. Straatsma, J. Phys. Chem. **91**, 6269 (1987).
[21] O. Steinhauser, Mol. Phys. **45**, 335 (1982).
[22] P. V. Hobbs, *Ice Physics* (Clarendon, Oxford, 1974).
[23] R. Biswas, G. S. Grest, and C. M. Soukoulis, Phys. Rev. B **38**, 8154 (1988).
[24] H. J. C. Berendsen, J. P. M. Postma, W. F. van Gunsteren, A. DiNola, and J. R. Haak, J. Chem. Phys. **81**, 3684 (1984).
[25] M. P. Allen and D. J. Tildesley, *Computer Simulation of Liquids* (Clarendon, Oxford, 1987).
[26] M. C. Bellissent-Funel, J. Teixeira, and L. Bosio, J. Chem. Phys. **87**, 2231 (1987).
[27] O. A. Karim and A. D. J. Haymet, J. Chem. Phys. **89**, 6889 (1988).
[28] Th. A. Weber and F. H. Stillinger, J. Chem. Phys. **80**, 438 (1984).
[29] O. A. Karim, P. A. Kay, and A. D. J. Haymet, J. Chem. Phys. **92**, 4634 (1990).
[30] J. Ji and B. M. Pettitt, Mol. Phys. **82**, 67 (1994).
[31] R. Pletzer, Ph.D. thesis, Innsbruck, 1985.
[32] J. A. Ghormley and C. J. Hochnadel, Science **171**, 62 (1971).
[33] R. A. Kuharski and P. J. Rossky, J. Chem. Phys. **82**, 5289 (1985).
[34] F. H. Stillinger, Adv. Chem. Phys. **31**, 1 (1975).
[35] E. Davies and J. C. Dore (private communication), E. Davies, thesis, Kent, 1992.
[36] A. Geiger and P. Mausbach, in *Hydrogen-Bonded Liquids*, edited by J. C. Dore and J. Teixeira (Kluwer, Dordrecht, 1991).
[37] A. Geiger, F. H. Stillinger, and A. Rahman, J. Chem. Phys. **70**, 4185 (1979).
[38] H. E. Stanley, J. Teixeira, A. Geiger, and R. L. Blumberg, Phys. A **106**, 260 (1981).
[39] F. Sciortino and S. L. Fornili, J. Chem. Phys. **90**, 2786 (1989).
[40] F. H. Stillinger, Science **209**, 451 (1980).
[41] K. A. Motakabbir and M. Berkowitz, J. Phys. Chem. **94**, 8359 (1990).
[42] F. H. Stillinger and A. Rahman, J. Chem. Phys. **57**, 1281 (1972).
[43] M.-C. Bellissent-Funel, J. Teixeira, L. Bosio, and J. C. Dore, J. Phys. Condens. Matter **1**, 7123 (1989).
[44] D. M. Blakey and J. Dore (to be published).